Proc. of the Hydrogen and Metal Hydride Batteries Symp.
186th Meeting of the Electrochemical Society, Miami Beach, FL,
Oct. 9-14, 1994.

BNL-60541
CONF-941063--14

Effect of Ce Composition on the Structural and Electronic Characteristics of some Metal Hydride Electrodes: A XANES and EXAFS Investigation

S.Mukerjee, J. McBreen, J. J. Reilly, J. R. Johnson and G. Adzic
Department of Applied Sciences
Brookhaven National Laboratory
Upton, NY 11973

M. P. S. Kumar, W. Zhang and S. Srinivasan
Center for Electrochemical Systems and Hydrogen Research
Texas Engineering Experiment Station
Texas A&M University
College Station, Texas 77843

ABSTRACT

Substitution of the B component in the prototype AB_5 type ($LaNi_5$) metal hydride alloys have resulted in their increased acceptance as anodes for rechargeable alkaline batteries. Recently substitution of the A component (La) for imparting properties such as increased corrosion resistance has recieved attention. This investigation deals with the role of Ce as a substituent for the La and its effect in terms of corrosion resistance. The alloys chosen have the general composition of $La_xCe_{1-x}B_5$ (x = 1, 0.8, 0.5 and 0.25) where B is $Ni_{3.55}Co_{0.75}Mn_{0.4}Al_{0.3}$ together with alloys containing the mischmetal (Mm) as the A component (both synthetic and commercial). Electrochemical cycling results show that Ce lowers the capacity loss in the alloys and that this effect is not a simple function of the extent of lattice expansion during hydriding as was previously suggested. Correlation of the electrochemical and XAS results show that capacity loss is directly related to the extent of Ni corrosion. Effect of Ce substitution seems to result in a stable Ce oxide hydroxide coating which imparts the corrosion resistance.

INTRODUCTION

Recent advances in the development of advanced nickel metal hydride alloys have resulted in it replacing cadmium as the anode in rechargeable alkaline batteries (1). Among the principle alloy types currently under consideration are the AB_2 and AB_5 type alloys. The hydrogen storage and electrochemical characteristics of these alloys depend intimately on their composition. Among the AB_5 type alloys, substitution of the prototype alloy $LaNi_5$ with small amounts of other alloying elements have shown improvements in terms of both electrochemical capacity as well as cycle life of the alloy material. A previous investigation (2) involving individual substitutions of Ni (in $LaNi_5$) with small amounts of Co, Al and Mn have shown their ability to improve the electrochemical capacity. These

improvements have been attributed to the lowering of the hydrogen plateau pressure. Recent results with Sn substitution (3,4) and have shown similar effects and have attributed the lowering of the hydrogen plateau pressure to an increase in the lattice parameters (cell volume). Such Ni substitutions also result in the decrease of the capacity loss due to lower corrosion. This has been attributed (5) to the reduced alloy expansion and contraction in these alloys (lower hydrogen molar volume). Similar effects are also observed as a result of substitution of La with rare earth elements such as Ce. This is borne out by the good performance characteristics of mischmetal $(Mm)B_5$ battery electrodes, wherein the Mm contains (in atom %) 50-55% Ce, 18-28% La, 12-18% Nd, 4-6% Pr, <0.1% Sm and <2% others. However little is known about the effect of Ce substitution in terms of its effect on the corrosion of individual alloying elements (particularly Ni) as a function of cycling.

X-ray absorption spectroscopy (XAS) can in principle elucidate both electronic and structural changes that occur on the substitution of alloy substituents and on the ingress of hydrogen into the alloy. The XAS spectra consists of two parts, the near edge part, XANES, which gives chemical information and the EXAFS which yields structural information. The X-ray absorption near edge structure (XANES, ± 50 eV relative to the absorption edge) comprises primarily of multiple scattering and transitions to empty states in the vicinity of the Fermi level by low energy photo-electrons with relatively long mean-free paths. The XANES can provide information on the oxidation state from the size and shift in the edge-transition, and on the coordination symmetry of ligands around the excited atom from the shape of the edge transition. The XANES probes empty states which are thought to be important in hydrogen storage (6). Due to its ability to probe empty states near the Fermi level it can provide important information on the extent of corrosion of individual components. The extended X-ray absorption fine structure (EXAFS) region is 40-1500 eV beyond the absorption edge and is caused by the modulation of the X-ray intensity due to back-scattering by a small fraction of the back-scattered photoelectron wave due to atoms surrounding the absorber. This interference effect caused by single-scattering electrons with short mean-free paths provides information about the short-range atomic order (coordination number and bond distances).

Recent results (7) have shown the possibilities of using *in-situ* XAS techniques to probe the individual components in terms of the structural, electronic and the corrosion characteristics of individual alloying elements. This investigation has shown that substitution of Ni and La by Sn and Ce respectively results in changes in the lattice parameters (both Ni-Ni and Ni-La distances) as well as partial filling of the Ni *d* states or lattice distortions causing changes in the coordination symmetry. There was also evidence indicating increase in the number of empty La *d* states. This study also indicated that electrochemical charge and discharge cycles result in Ni corrosion. There was also evidence indicating the ability of Ce to impart corrosion resistance when used as a substituent for La.

This investigation therefore aims to investigate the effect of Ce composition as a substituent for La in a series of metal hydride alloys where the B component remained unchanged. The composition of component B ($Ni_{3.55}Co_{0.75}Mn_{0.4}Al_{0.3}$) was based on those

DISCLAIMER

Portions of this document may be illegible in electronic image products. Images are produced from the best available original document.

commonly used as AB_5 battery electrodes. Besides these, alloys containing Mm (both synthetic as well as those commercially available prepared from Bastnasite ore) as component A were also used. The principle effort therefore was to investigate the effect of Ce composition in terms of corrosion characteristics of individual alloying components, primarily the Ni.

EXPERIMENTAL

The alloy compositions were LaB_5, $La_{0.8}Ce_{0.2}B_5$, $La_{0.5}Ce_{0.5}B_5$, $La_{0.25}Ce_{0.75}B_5$ and MmB_5 (both synthetic and commercial) where B_5 is $Ni_{3.55}Co_{0.75}Mn_{0.4}Al_{0.3}$. The composition of the synthetic Mm alloy was chosen to be (in atom%) 26% La, 52% Ce, 16% Nd and 6 % Pr. All the alloys were prepared using the arc melting technique and were annealed at 1173°K for 3 days. The details of the preparation conditions used together with the methodology for determination of the P-C-T isotherms, the molar volume of hydrogen in the hydride phase and the X-ray diffraction analysis is given elsewhere (8). Electrodes prepared from a portion of each alloy (73 mg) were subjected to electrochemical cycling using a computer controlled battery cycler (Arbin Corp., College Station, Texas). The charging rate used was 10 mA for 3 hours (2.5 hours for alloys possessing below 300 mAh/gm capacity). The cutoff voltage for the discharge cycle was -0.7 V vs. Hg/HgO reference electrode. The electrode composition used for these tests were in the weight ratio of 17% Teflon, 33% carbon black (Vulcan XC 72) and 50 % alloy. All electrochemical cycling measurements were conducted in a flooded vented cell in 6 M KOH electrolyte. Details of the electrode preparation and testing are given elsewhere (7-9). After 100 cycles the electrode material was removed from the current collector, washed with deionized water to remove KOH and ultrasonically dispersed in acetone. After drying, these material were mixed with BN and pressed into pellets for *ex-situ* XAS studies. The electrodes for the XAS measurements were thin discs (0.25 mm thick and 19 mm in diameter) that comprised of the alloy, carbon black (Vulcan XC-72), vitreous carbon fibers and a polyvinylidine fluoride binder. They were prepared using a standard vacuum table paper making technique (10). Prior to electrode fabrication, all the alloys were activated by subjecting each to several hydriding-dehydriding cycles in the Sievert's apparatus. This produces a fine powder that eliminates thickness effects in the EXAFS and avoids the need for an electrochemical activation procedure. For detailed accounts of the activation procedure see refs., 11-12. The metal hydride electrodes for the *in-situ* studies were charged at a constant current of 3mA for 7 hours and discharged at a current of 5mA to a potential of -0.7 V vs. Hg/HgO reference electrode. The charging rate allowed for considerable overcharge because the electrodes contained only $\approx$ 50 mgs of the alloy. XAS scans for the hydrided samples were run after subjecting the electrodes for five charge discharge cycles and were conducted within 30 minutes of termination of charge.

The X-ray absorption spectroscopic (XAS) measurements were conducted at the Beam Lines X23A2 and X11A at the National Synchrotron Light Source (NSLS). Details of the monochromator design, detuning, and energy resolution of the respective Beam Lines are given in detail elsewhere (10, 13-14). XAS measurements were made in the transmission mode, at the La L_3, Ni K and Ce L_3 edges, before and after electrochemical

cycling (100 times) and as a function of electrochemical charging. The data acquisition for XAS comprised of three ionization detectors (incidence I_o, transmittance I_t, Reference I_{ref}). The reference channel was primarily for internal calibration of the edge positions and was used in conjunction with pure foils or oxide samples of the respective elements. For the Ni K edge pure N_2 was used in all the chambers, while for the La/Ce L_3 edges a mixture of 80%He and 20%N_2 was used in the incidence chamber while passing pure N_2 in the transmittance and reference chambers. The data analysis package used for the XANES analysis was the University of Washington analysis program (15). The data analysis was done according to procedures described in detail elsewhere (10,13-14,16-17). The EXAFS data analysis used computer algorithms developed by Koningberger and coworkers (15-17). The Fourier filtering and analysis of the EXAFS spectra were conducted according to procedure described in detail elsewhere (10,13-14).

RESULTS AND DISCUSSION

X-ray Diffraction and Electrochemical Characterization

Table 1 shows the results of electrochemical and X-ray diffraction analysis. As evident from these results, addition of Ce causes a significant lowering in capacity loss with cycling. Comparison of the cell volume expansion due to hydriding for LaB_5 and $La_{0.8}Ce_{0.2}B_5$ shows similar behavior, which suggests that corrosion resistance imparted due to addition of Ce cannot be simply related to the extent of lattice expansion and contraction as suggested Willems and Buschow (5). As pointed out by Adzic et al., (this conference, (8)), addition of Ce results in higher initial capacity and hence an increase in the number of hydrogen atoms per unit cell. However, as shown in ref. (8), further increase in the Ce composition (beyond 0.2) causes a decrease in the cell volume (due to the smaller size of Ce) which results in higher hydrogen plateau pressure and hence lower charging efficiencies. These are manifested in lower initial capacity and number of hydrogen atoms per unit cell. As a result, the volume expansion due to the hydriding process is lower and this could be a further contributing factor in lower capacity loss, with higher Ce content. The MmB_5 prepared using commercially available Mm had the lowest capacity loss, even less than that for the synthetically prepared analogue. This behavior could be partly explained on the basis of lower cell volume and more importantly lower cell volume expansion as a consequence of hydriding as compared to the synthetic analogue. Similar electrochemical characteristics (capacity loss, initial capacity number of hydrogen atoms per unit cell etc.) for both synthetic MmB_5 and $La_{0.5}Ce_{0.5}B_5$, both of which possess similar Ce content (~50 atom%) implies that Ce is the prime contributor to corrosion resistance.

XAS results at the Ni K edge

Figure 1 shows the normalized Ni K edge XANES spectra for dry uncycled LaB_5, $La_xCe_{1-x}B_5$ (X=0.8, 0.5 and 0.25) and MmB_5. The XANES for all the electrodes exhibit a small pre-edge peak which can be ascribed to *p-d* hybridization, allowing transitions into the empty 3*d* states of Ni. As shown previously (6-7) such mixing of *p-d* states is expected, based on the hexagonal symmetry of the lattice. However as shown in figure 1 there is no effect on the pre-edge peak as a function of Ce composition, implying minimal distortions in lattice symmetry due to incorporation of Ce. Figure 2 shows the normalized

Ni K edge XANES spectra for LaB_5 before and after electrochemical cycling (100 times) together with that of a dry β-$Ni(OH)_2$ electrode. Appearance of a white line for the cycled LaB_5 electrode indicates corrosion of the Ni surface. Comparison of the area under this peak with that for the β-$Ni(OH)_2$ was used to estimate the degree of corrosion. It indicates that 18% of the Ni has corroded (Table 2). Figure 3 compares the white lines for LaB_5 and $La_{0.8}Ce_{0.2}B_5$ after 100 cycles with that for a dry β-$Ni(OH)_2$ electrode. As evident from this figure, the addition of Ce, significantly lowers the Ni corrosion to 8% after 100 cycles (Table 2). Figure 4 shows a similar comparison of the XANES for uncharged dry MmB_5 electrode and an electrode after 100 cycles (both synthetic and commercial). The lack of white line indicates that there was almost no corrosion of the MmB_5 prepared from commercially available Mm ore. Compared to this, the synthetically prepared sample exhibited slightly higher Ni corrosion. As mentioned previously, this difference could be partly explained on the basis of lower lattice expansion in the case of the commercial Mm sample. The extent of Ni corrosion determined from comparison of the white line in the Ni K edge for the cycled MmB_5 samples are given in Table 2. These differences in the Ni corrosion can also be observed in the EXAFS region at the Ni K edge. Figure 5 shows the Fourier transforms of the EXAFS at the Ni K edge for LaB_5 before and after 100 cycles. The main peak centered around 2 Å contains contributions from Ni-Ni interactions from both the basal plane (plane containing both A and B components) and those in between the basal planes containing exclusively the B component. Besides these there are the smaller interaction from Ni-La and Ni-M (where M denotes all the Ni substituents). Comparison of the cycled and uncycled spectra shows formation of peaks around 1.5 Å for the cycled sample and a consequent lowering of the Ni-Ni interactions which could be accounted for, due to the formation of nickel oxides on the cycled electrodes. The absence of these oxides on the uncycled electrodes shows that no nickel oxidation occured in preparing these alloy electrodes. Figure 6 show a similar comparison of the Fourier transform of the Ni K edge EXAFS for $La_{0.8}Ce_{0.2}B_5$. This figure shows evidence for the formation of oxides on the Ni surface on the cycled electrode and its absence in the uncycled ones. Comparison with similar spectra obtained for LaB_5 shows that the extent of this oxide formation after 100 cycles was lower in the sample containing Ce.

XANES Results at the Ce L_3 edge

Figure 7 shows the XANES spectra at the Ce L_3 edge for $La_{0.8}Ce_{0.2}B_5$ as a function of charge and discharge. As evident from this figure, the electrode in its dry uncharged virgin state possesses Ce in a mixed +3/+4 valence state. This is in agreement with previous results on intermettalic alloys containing Ce (18-19). There is however a change in the oxidation state of Ce to +3 state as a result of hydriding. This is consistent with previous results of Garcia *et. al.*, which involved the $CeRu_2$ and $CeFe_2$ alloys, with hydriding conducted in the gas phase (18). The effect of discharge, is reversion to the mixed +3/+4 state. The increase in the XANES peak at 13 eV in the discharged electrode after 100 cycles indicates some Ce oxidation (fig. 7). Figure 8 shows the analogous XANES spectra for the MmB_5 alloy exhibiting similar effect of oxidation state change during the charging process and its reversion during discharge. The effect of electrochemical cycling however indicated much lower corrosion of the Ce as compared to

$La_{0.8}Ce_{0.2}B_5$. This effect was same for both high purity as well as the commercially obtained Mm sample. There also seems to be a direct relation between the magnitude of the white line in the case of Ce in the +3 state (charged electrode) and the hydrogen uptake by the respective alloy. This was confirmed from similar XANES analysis on the other alloy electrodes with different Ce contents ($La_xCe_{1-x}B_5$, with X=0.5 and 0.25).

Ce is a well known corrosion inhibitor for both steel and aluminum (20). The corrosion inhbition properties may be due to the formation of a stable CeO_2 layer. A similar mechanism may be operative in the case of AB_5 hydrides. Further work is neccessary to elucidate the role of Ce in lowering the corrosion rate on cycling.

CONCLUSIONS

Based on the results of this study, there is evidence of a direct correlation between the electrochemical stability imparted as a result of addition of Ce (as a substituent to La) and Ni corrosion in the alloy. However, since addition of Ce causes a small degree of lattice contraction (due to the smaller size of Ce as compared to La) its addition beyond ~ 20% causes lowering of the hydrogen uptake and hence electrochemical capacity. In this context it is interesting to note that the synthetic Mm alloy had similar corrosion resistance to the $La_{0.5}Ce_{0.5}B_5$ alloy (both possessing similar Ce content). This was also reflected in the similar extent of Ni corrosion after 100 cycles. The commercial Mm alloy however had a much lower capacity loss and a consequently lower Ni corrosion which could be attributed to the presence of other elements such as Sm, in small amounts as well as the much lower volume expansion during the hydriding process. Results from the XANES analysis at the Ce L_3 edge shows that Ce is present in a mixed +3/+4 state in the unhydrided state and shifts to +3 state during the hydriding step. The formation of a stable Ce rich oxide hydroxide layer on the alloys could account for the improved corrosion resistance of these alloys.

ACKNOWLEDGMENTS

This work was supported by the Chemical Science Division, Office of Basic Energy Sciences, U. S. Department of Energy, under contract No. DE-AC02-76CH00016. We would like to acknowledge the support of the Department of Energy, Division of Material Science (contract # DE-AC02-76CH00016) for its role in the development and operation of the National Synchrotron Light Source (NSLS).

REFERENCES

(1) J. J. Reilly, in *Hydrogen Storage Materials, Batteries and Electrochemistry*, (D. A. Corrigan and S. Srinivasan, Eds.,) The Electrochemical Society Inc., **92-5**, 24, (1992)

(2) T. Sakai, K. Muta, H. Miyamura, N. Kuriyama and H. Ishikawa, *in Hydrogen Storage Materials, Batteries and Electrochemistry* (D. A. Corrigan and S. Srinivasan, Eds.,) The Electrochemical Society Inc., **92-5**, 59, (1992)

(3) J. S. Cantrell, T. A. Beiter and R. C. Bowman Jr., *J. Alloys and Compounds*, **207-208**, 372, (1994)

(4) B. V. Ratnakumar, S. Surumpudi, S. Di Stefano, G. Halpert, C. Witham and B. Fultz, *186th Meeting of the Electrochemical Society*, Miami Beach, Oct. 9-14, 1994, **94-2**, 56, (1994)

(5) J. J. G. Willems and K. H. J. Buschow, *J. Less Common Metals*, **129**, 13, (1987)
(6) M. Gupta, L. Schlapbach, *Hydrogen in Intermettalic Compounds-I* (L. Schlapbach, Ed.,), Topics in Physics Series, Springer Verlag, **63**, 139, (1988)
(7) S. Mukerjee, J. McBreen, J. J. Reilly, J. R. Johnson, G. Adzic, K. Petrov, M. P. S. Kumar and S. Srinivasan, *J. Electrochem. Soc.*, Submitted, 1994
(8) G. D. Adzic, J. R. Johnson, J. J. Reilly, J. McBreen and S. Mukerjee, (This Journal)
(9) K. Petrov, A. A. Rostami, A. Visintin and S. Srinivasan, *J. Electrochem. Soc.*, **141**, 1747, (1994)
(10) J. McBreen, W. E. O'Grady, K. I. Pandya, R. W. Hoffman and D. E. Sayers, *Langmuir*, **3**, 418, (1987)
(11) J. J. Reilly, in *Inorganic Synthesis* (S. L. Holt Ed.,) J. Wiley & Sons, New York (1983), p 90
(12) M. H. Mendelsohn, D. M. Gruen and A. E. Dwight, *ibid*, p96
(13) S. Mukerjee, J. McBreen, S. Srinivasan and M. P. Soriaga, *J. Electrochem. Soc.*, (in press)
(14) K. I. Pandya, R. W. Hoffman, J. McBreen and W. E. O'Grady, *J. Electrochem. Soc.*, **137**, 383, (1990)
(15) D. E. Sayers, D. A. Bunker, in *X-ray Absorption: Principles, Applications Techniques of EXAFS, SEXAFS and XANES*, (D. C. Koningsberger and R. Prins, Eds.,) John Wiley & Sons, New York, p 211, (1988)
(16) J. Wong, F. W. Lyttle, R. P. Messner, D. H. Maylotte, *Phys. Rev. B.*, **30**, 5596, (1984)
(17) J. B. A. D. van Zon, D. C. Koninsberger, H. F. I. vant'Blik and D. E. Sayers, *J. Chem. Phys.*, **82**, 5742, (1985)
(18) J. Garcia, J. Bartolome, M. S. del Rio, *Zeitschrift fur Physikalische Chemie Nue Folge, Bd.*, **163**, S 277 (1989)
(19) G. Krill, *J. Phys.*, **C8**, 907, (1986)
(20) A. J. Davenport, H. S. Isaacs and M. W. Kendig, *Corrosion Science*, **32**, 653, (1991)

DISCLAIMER

Table 1

Results of X-ray diffraction and electrochemical characterization as a function of Ce composition.

Composition	n* # of H atoms/Cell	Cell Volume $(Å)^3$	Initial Capacity mAh/g	Capacity Loss mAh/g cycle
LaB_5	4.8	89.56 (108.56)†	316	0.41
$La_{0.8}Ce_{0.2}B_5$	5.4	88.84 (107.84)†	327	0.21
$La_{0.5}Ce_{0.5}B_5$	4.3	87.33 (104.79)†	278	0.15
$La_{0.25}Ce_{0.75}B_5$	1.3	86.19 (95.16)†	83	-
MmB_5 (synthetic)	4.3	87.39 (101.65)†	283	0.22
MmB_5 (commercial)	3.6	86.27 (97.07)†	231	0.08

* Based on initial electrochemical capacity after activation and one formula unit per unit cell, i.e., AB_5H_n

† Volume measured after gas phase hdyriding.

Table 2

Extent of Ni Corrosion determined from XANES analysis. The degree of corrosion was estimated from the area under the white line.

Alloy Composition	Extent of Ni Corrosion (%)
LaB_5	18
$La_{0.8}Ce_{0.2}B_5$	8
$La_{0.5}Ce_{0.5}B_5$	5
MmB_5 (Synthetic)	4
MmB_5 (Commercial)	2

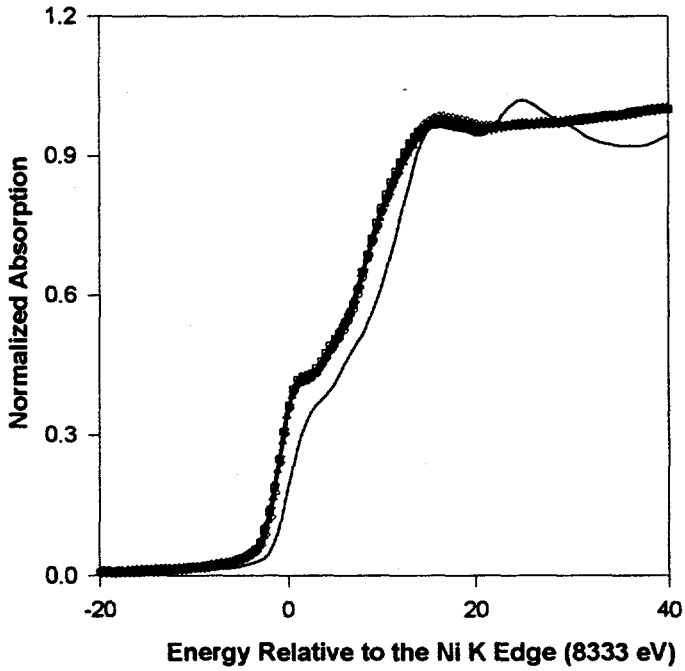

Figure 1. Ni K edge XANES for dry uncharged electrodes. Ni foil (—), LaB_5 (□), $La_{0.8}Ce_{0.2}B_5$ (○), $La_{0.5}Ce_{0.5}B_5$ (▽), $La_{0.25}Ce_{0.75}B_5$ (△) and MmB_5 (◇).

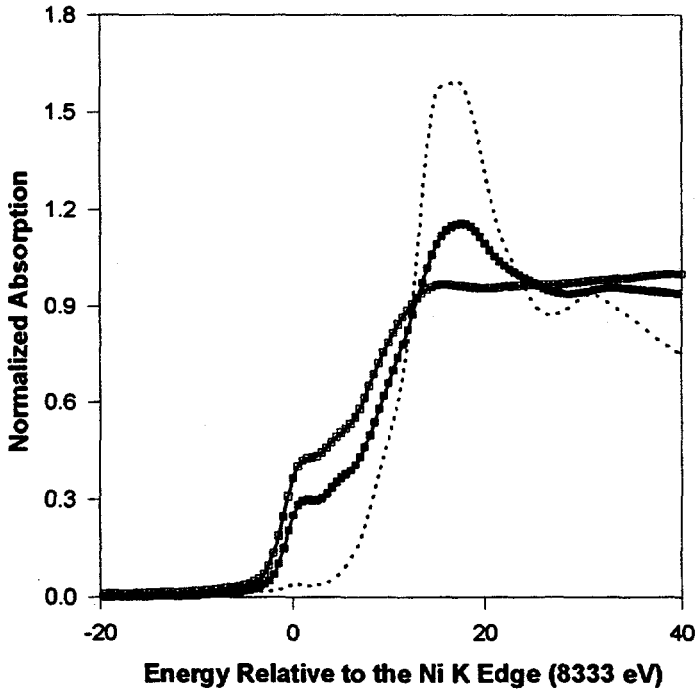

Figure 2. Ni K edge XANES for LaB_5 electrode before and after cycling. $Ni(OH)_2$ (....), Uncycled LaB_5 (□), LaB_5 after 100 cycles (■).

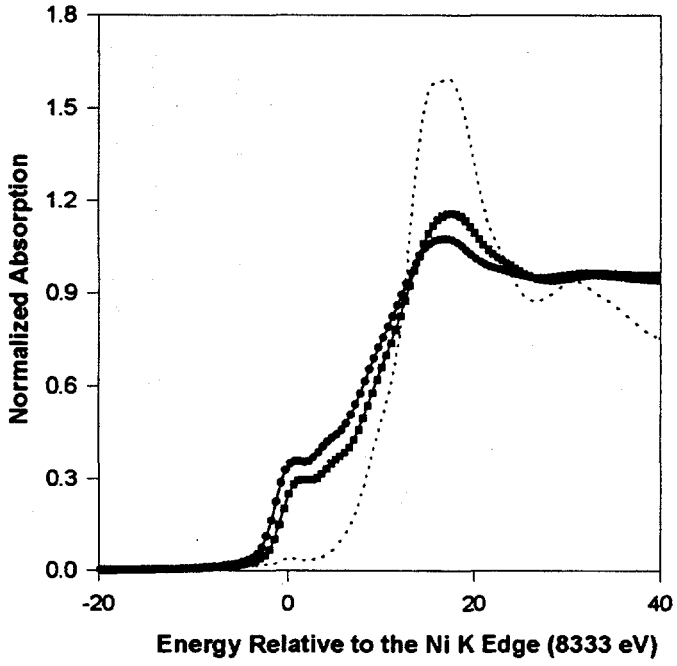

Figure 3. Ni K edge XANES for electrodes after 100 cycles. LaB_5 (■), $La_{0.8}Ce_{0.2}B_5$ (●) and $Ni(OH)_2$ (...).

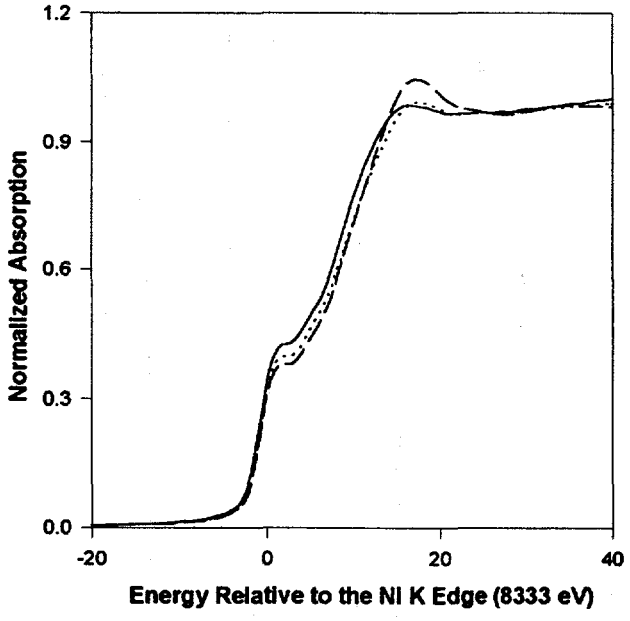

Figure 4. Ni K edge XANES for MmB_5 electrodes (commercial and synthetic) after 100 cycles. MmB_5 (uncycled) (—), MmB_5 (commercial) (...) and MmB_5 (synthetic) (---).

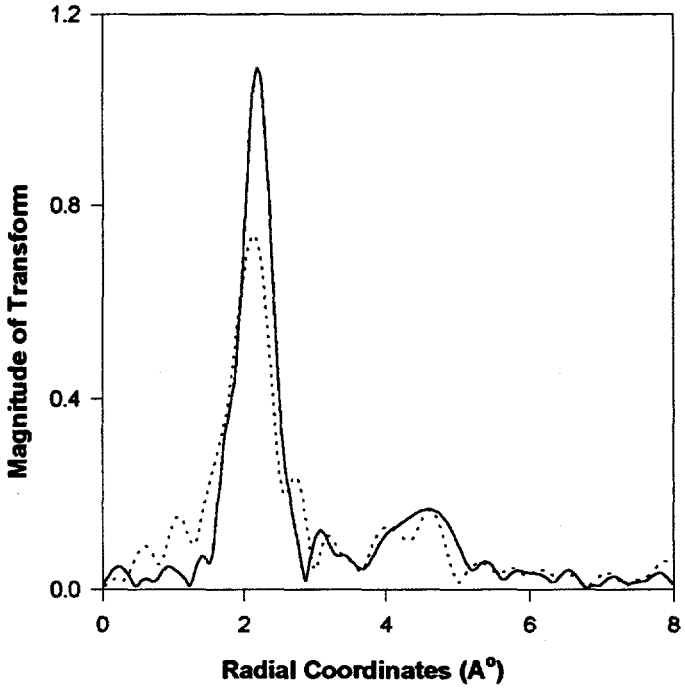

Figure 5. EXAFS at the Ni K edge for LaB_5 electrode before (—) and after 100 cycles (....).

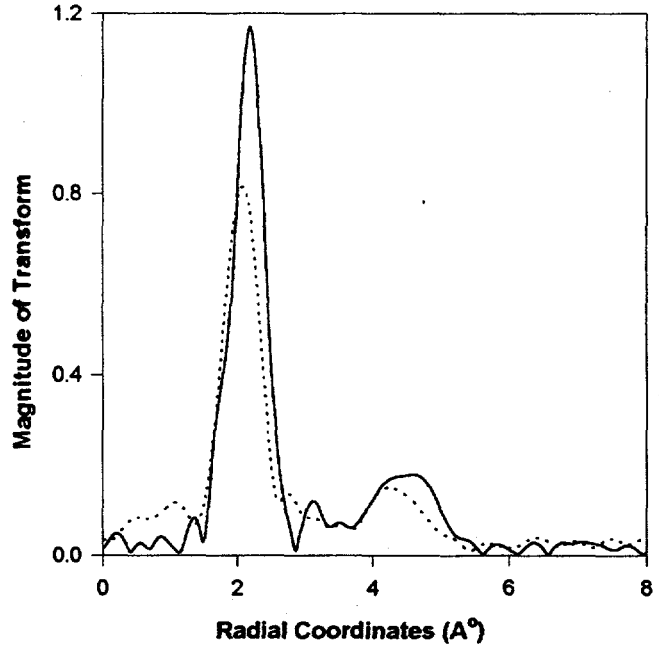

Figure 6. EXAFS at the Ni K edge for $La_{0.8}Ce_{0.2}B_5$ electrode before (—) and after 100 cycles (....).

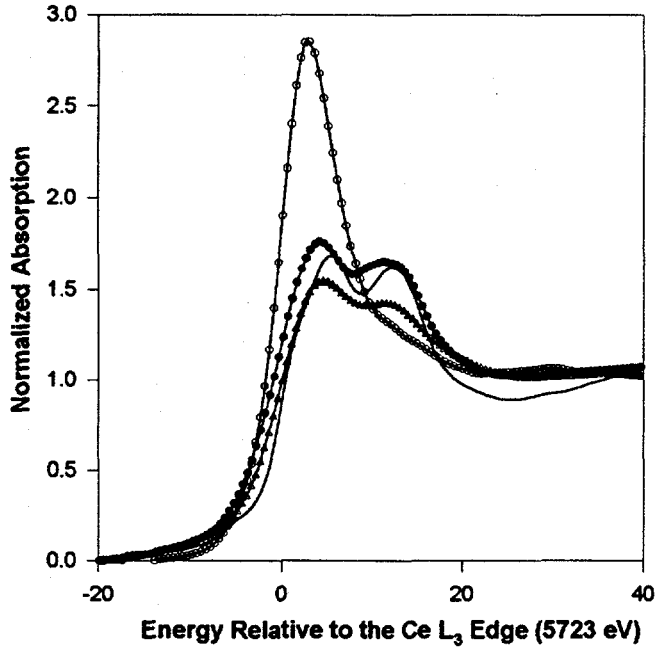

Figure 7. Ce L_3 XANES for $La_{0.8}Ce_{0.2}B_5$ as a function of charge and discharge after 100 cycles. CeO_2 reference standard (—), $La_{0.8}Ce_{0.2}B_5$, dry uncharged (Δ), charged (O) and discharged after 100 cycles (●).

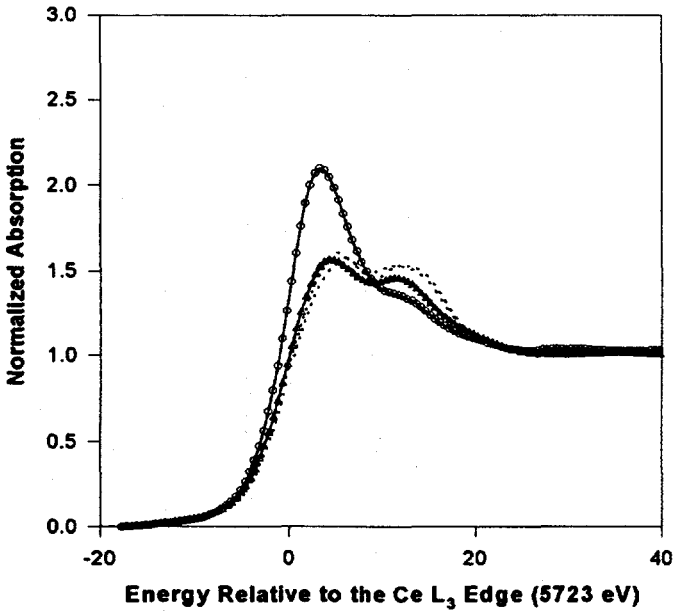

Figure 8. Ce L_3 XANES for MmB_5 as a function of charge and discharge after 100 cycles. MmB_5, dry uncharged (Δ), charged (O) and discharged after 100 cycles (both commercial and synthetic) (...).

SHORT ABSTRACT

Metal Hydrides are increasingly being accepted as anode electrodes of choice for rechargeable alkaline batteries. However, scope exists for further improvements in both capacity as well as cycle life of the hydride electrodes. Application of X-ray absorption techniques (XAS) of XANES and EXAFS has the ability to probe these materials with element specificity and *in-situ* capability to provide information on both electronic, structural and corrosion characteristics. This paper will present the application of XAS in the study of some metal hydride electrodes as a function of charge, discharge and cycling.